Hydrogeological and Geoelectrical Prospecting for Groundwater within parts of Northeastern Bosso, North-central Nigeria

Christopher Unuevho
Federal University of Technology Minna

Amadi Akobundu Nwanosike
Federal University of Technology Minna

HYDROGEOLOGICAL AND GEOELECTRICAL PROPECTING FOR GROUNDWATER WITHIN PARTS OF NORTHEASTERN BOSSO, MINNA, NORTH-CENTRAL NIGERIA REGION

Unuevho, C.[1], Onuoha, K.M.[2], Ogunbajo, M.I.[1], Amadi, A.N.[1]

[1]DEPT OF GEOLOGY, FEDERAL UNIVERSITY OF TECHNOLOGY, MINNA
[2]DEPT OF GEOLOGY, UNIVERSITY OF NIGERIA, NSUKKA

[1]Correpondening author's e-mail: unuevho@gmail.com

ABSTRACT

This work employed static water elevation data to delineate areas where hand-dug wells are seasonally productive from areas where they are continually productive in parts of northeastern Bosso, Minna. It also integrated low resistivity anomaly with data on electrical anisotropy, longitudinal unit conductance and transverse unit resistance to identify areas with deep water-bearing fractures. A large number of boreholes have been completed in the shallow fractures, and this has resulted in seasonal production from the shallow aquifers. Hand-dug wells within the groundwater convergence zone established in this work were found to produce water continually, while those located around the established groundwater level ridges are seasonally productive. The groundwater convergence was found to exist within the central portion of the study area, where the work revealed high surface fracture density values (2.4 to $3.0m^{-1}$) and surface fracture permeability values (0.0003 to $0.00046m^2$). Deep fractures with optimum attributes for water production were found in the north-western and north-eastern portions of the study area, within latitudes N9.645° to N9.665°.

INTRODUCTION

The study area is within northeastern Bosso, an urban sprawl settlement in northern part of Minna (Niger State capital in Nigeria, Figures 1 and 2). It is enclosed within geographic coordinates N9°31'32.9" to N9°39'41.4" and E6°30'43.8" to E6°34'42.8". The residents here are an admixture of low social class people (mainly petty traders and peasant farmers) and lower middle class people, mostly employees of the Federal University of Technology, Minna (FUTMINA). Pipe-borne water system here functions very poorly, and the residents often obtain potable water from hand-dug wells and hand-pumped boreholes. Many of the hand-dug wells become dry from middle January to the end of Dry season in middle April. This happens when wells are sited close to static groundwater level ridge, commonly called groundwater divide. This is the linear axis from which groundwater diverges away in opposite directions. It is also known as the recharge zone. The area is also noted for significant failure rate of bore-holes drilled with mechanised drilling rigs. Eight wells were drilled within the oppositely adjacent FUTMINNA's Bosso campus. Three of these were outright failure, while three provide potable water only from May to early January. These wells are hand-pumped, which implies they were completed in aquifers constituted by fractures that are shallower than 50m. Crowded production from shallow fractures would lead to well failure or seasonal production.

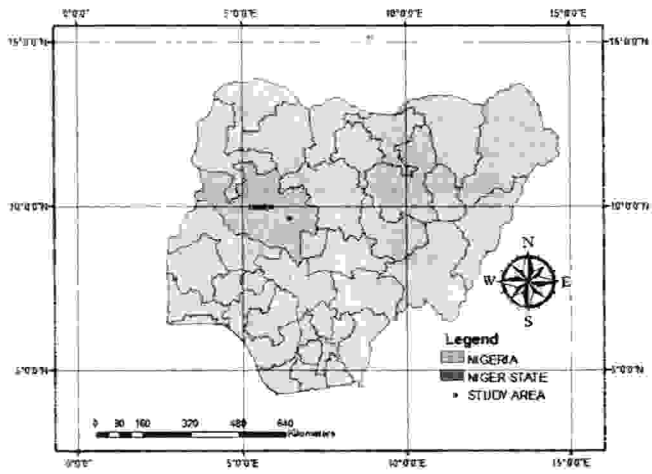

Figure.1. Map of Nigeria showing study area within Niger State

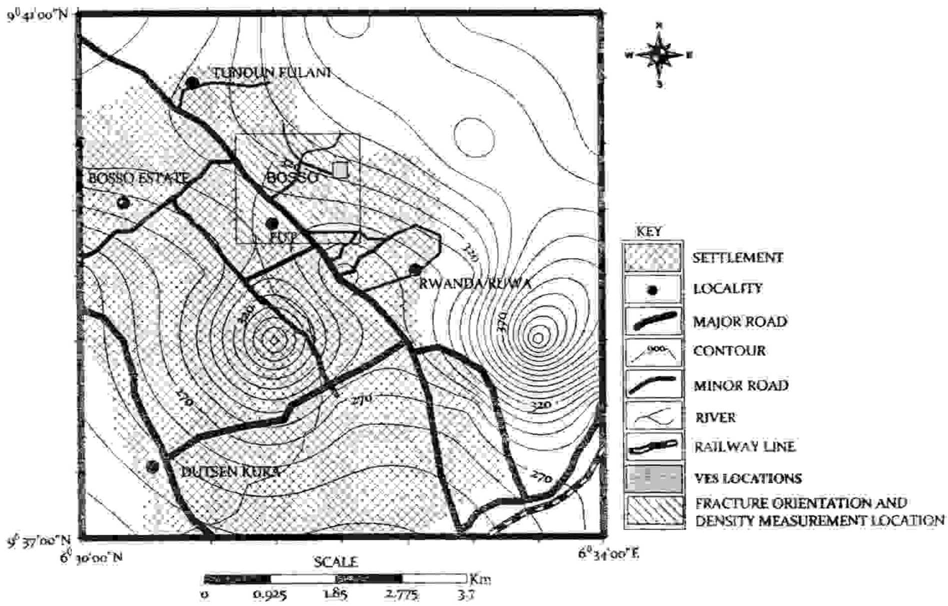

Figure 2. Location of study area within NE Bosso

The unsatisfactory well performance may also result from non-deployment of appropriate geo-scientific procedures when positioning hand-dug wells and boreholes in the study area, which is a basement complex where aquifers localized and compartmentalized (Sonkambe *et al.* 2013). The orthodox method deployed to site water wells in these areas employs Vertical Electrical Sounding (VES) to delineate subsurface zones with anomalous low resistivity values, which are attributed to the presence of groundwater. The flaw in this method is that the presence of clay minerals (such as chlorite, thuringite , clinochlore and dickite) and other electronically conductive minerals (for example, galena, graphite, chalcopyrite, native copper and gold) in basement complex rocks will produce similarly anomalous low resistivity values, and therefore misdirect well positioning exercise. Positioning water wells is essentially a geological problem (Bhattachayra and Patra, 1968) because groundwater occurrence is controlled by geology. The success of groundwater prospecting in the basement complex areas depends upon an appropriate combination of physics and geology (Paranis, 1986) with reliable information on hydrogeological characteristics (Chandra *et al.*, 2006). Oyedele *et al.* (2013) employed electrical resistivity sounding (VES) data to delineate fractured basement intervals depressions within parts of Ado-Ekiti in SW Nigeria. Electrical anisotropy (λ), longitudinal unit conductance(S) and transverse unit resistance (T) derived from VES data are hydrogeological parameters related to degree of fracturing, fracture permeability and groundwater occurrence (Olorunfemi and Oloruniwo, 1985; Olorunfemi *et al.*,1991; Sunmonu *et al.*,2012; Kumar *et al.*,2014). Groundwater converging centres are first choice zones for positioning water wells (Olorunfemi and Idornigie, 1992; Mallam and Emenike, 2008; Unuevho *et al.*2008).

AIM AND OBJECTIVES

The aim of this work was to employ direct geological and hydro-geological data to establish groundwater flow directions and groundwater convergence zones in the regolith, as well as to employ geophysical data to delineate deep water-bearing fractures in the study area. The associate objectives were to generate surface fracture density and permeability maps, static water level elevation map, isoresistivity map as well as thickness map, longitudinal unit conductance

(S) map, transverse unit resistance (T) and coefficient of electrical anisotropy (λ) maps for deep aquifers (constituted by fractures within 50-70m; and 70-90m) in the study area.

GEOLOGY AND HYDROGEOLOGY OF THE AREA

Outcrop lithology in the study area is medium to coarse grained granite. Fine grained granite outcrops on its west while schist-migmatite-gneiss complex outcrops northwards of it (Fig.3). Figures 4 and 5 are some of the widespread surface fractures in the area.

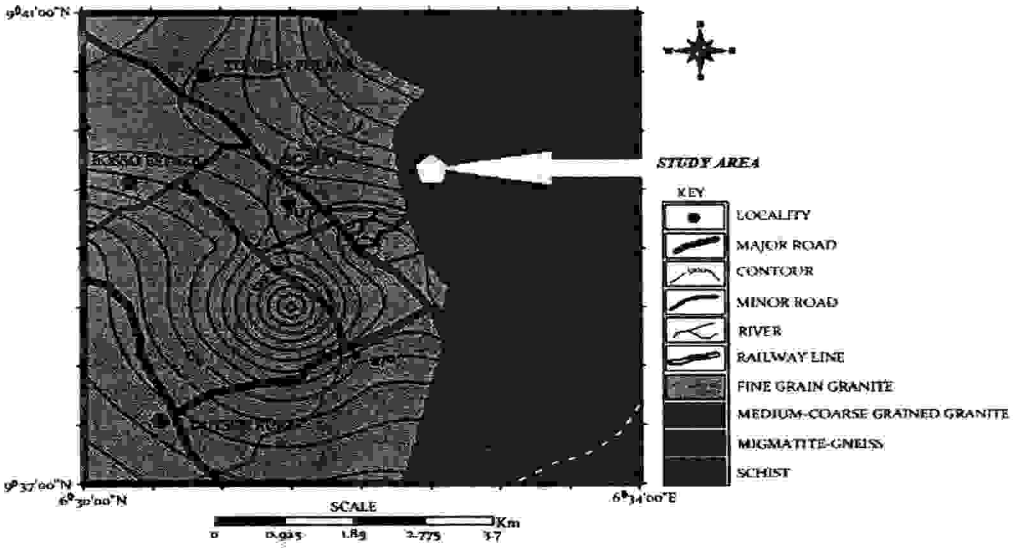

Figure 3. Geologic map of the study area

Figure 4. Surface interconnected fractures at N09°39'.520''; E006° 31'.762''

Figure 5. Surface interconnected fractures at N09°39'.402''; E006° 31'.489''

Aquifers in the area comprise regolith, unconfined and confined fractures, as is typical of the basement complex (Olorunfemi, 2009). The regolith is the clastic detritus produced from weathering of outcropping bedrocks. Petty traders, local farmers and lower middle class residents in the study area commonly obtain water from wells manually dug into the regolith. The unconfined fractures directly underlie the regolith. The confined fractures are sandwiched between fresh bedrock above and below. It takes mechanised drilling to bore a well through the fractures. The unconfined fractures are commonly shallower than 50m. They have become overexploited in the study area where over 90% of existing wells are hand-pumped. Some of the confined fractures are shallower than 50m, but majority of them are deep. Wells completed in deep fractures are productive in areas where shallow aquifer wells failed in Minna and Zungeru towns of Niger State. Figures 6 and 7 show water flowing within the fracture interval between first fresh basement layer (bedrock above) and second basement layer (bedrock below). Such confined fracture systems and unconfined fractures presumably exist within bedrock buried beneath regolith.

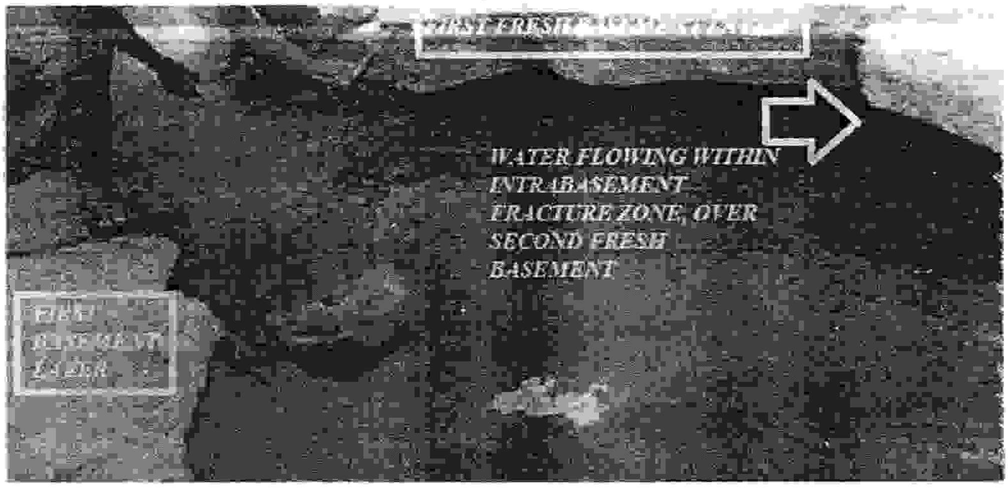

Figure 6. Water flowing within intra basement fracture zone at N09°39'.98''; E006° 31'.58''

Figure 7. Water flowing within intra basement fracture zone at N09°39'.96''; E006° 32'.00'

METHODOLOGY

Strike direction of surface fractures on outcrops was mapped using and compass clinometers and a Global Positioning System (GPS) tool. The strike directions of the fractures were plotted on a Rossette diagram using software called Rockworks. Surface fracture density was determined at different locations using:

$$F_d = \frac{N}{L} \quad \text{(Deming, 2002)} \qquad 1$$

where F_d N, L are surface fracture density (in m^{-1}), number of fractures and linear distance (in m) across fractures respectively. Fracture permeability at different locations was determined using:

$$F_k = \frac{F_d W^3}{12} \text{ (Deming, 2002; Brace, 1980) .... 2}$$

Where F_k, F_d, W are fracture permeability, fracture density and fracture width (in m) respectively. Static water level depth was determined at twenty four different locations, by lowering a water level indicator to the top of water level in the wells. This was subtracted from the elevation measurement of protective concrete structure atop each well (obtained with a GPS) to obtain water level elevation at each well location. Geographic coordinates of all the locations were determined with a GPS device. Contour maps of F_d, F_k and static water level values were generated using Suffer 11 contouring software. The ridge on the static water level (commonly called groundwater divide) and groundwater flow directions were established from the static water level elevation map. Closures of low contour values on the static water elevation contour map were inferred to be groundwater convergence zones (also known as groundwater discharge zones). VES data was acquired at twenty three different locations using the Schlumberger field array. The current electrode spacing was limited to 160m by random location of residential and commercial buildings. The data were interpreted in terms of geo-electric layers using Winresist. The geo-electric layers are soil, weathered basement, first fresh basement layer interval, second fresh basement, third fresh basement and fractured basement. Soil and weathered basement layers were combined as regolith. Fractures deeper than 50m were delineated as deep fractures. The fractures within 50-70m depth were grouped into one class. Those within 70-90m were grouped into another class. Another group of fractures lies within 85-120m. Most fractures within these groups of depth interval are expected to be the genetically related and therefore interconnected. They were characterised in terms of hydro-geologically significant physical quantities (total longitudinal unit conductance, S; total transverse unit resistance, T; and coefficient of electrical anisotropy, λ) that were determined as follows:

$$S = \frac{H}{\rho} \qquad \text{(Henriet, 1976)} \quad \ldots\ldots\ldots\ldots\ldots\ldots\ 3$$

$$T = \rho H \qquad \text{(Henriet, 1976)} \quad \ldots\ldots\ldots\ldots\ldots\ldots\ 4$$

$$\lambda = \frac{\sqrt{TS}}{H} \qquad \text{(Henriet, 1976)} \quad \ldots\ldots\ldots\ldots\ldots\ldots\ 3$$

Isoresistivity contour maps, thickness contour maps, as well as contour maps of S, T and λ were generated for the deep fractures using Suffer 11.

RESULTS AND DISCUSSION

The strike of the surface fractures measured on the outcrops is given as table 1.

Table 1: Measured strike of fractures

204, 260, 220, 60,90. 271, 246, 188, 204, 108,168, 188, 182, 43, 182, 82, 184, 200,280,148, 29, 47,352,40,4,340,272,200,301,273, 229, 180, 298, 161, 292, 104, 193, 240, 98, 212, 340, 184, 243,189, 220, 258, 291, 162, 303, 8

Rosette diagram of the fractures' strike values (Fig.8) indicates that the major fracture system in the area trends NNE-SSW.

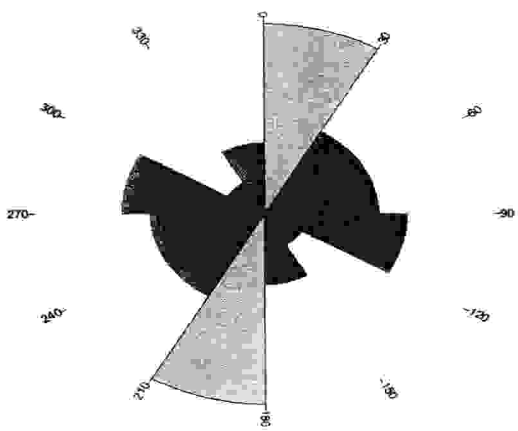

Figure 8. Rosette diagram of surface fractures' strike values

The estimated values of surface fracture density and permeability shown in table 2.

Table 2: Estimated of surface fracture density and permeability

LOCATION IDENTITY	NUMBER OF FRACTURES	LENGTH ACROSS FRACTURES	FRACTURE DENSITY	FRACTURE WIDTH	FRACTURE PERMEABILITY
L1	3	1.75	1.7	0.03	0.0000039
L2	3	1	3.0	0.07	0.0000086
L3	2	1.9	1.1	0.09	0.000067
L4	7	2.7	2.6	0.12	0.00039
L5	6	2	3.0	0.12	0.00043
L6	4	1.6	2.5	0.13	0.00046
L7	5	3.9	1.3	0.01	0000001
L8	8	3.4	2.4	0.01	0.0000002
L9	5	5.5	0.9	0.13	0.000017
L10	3	1.8	1.7	0.12	0.00024
L11	3	1.7	1.8	0.1	0.00015

The surface fracture density map (Fig.9) reveals that fracture density is higher in the central portion, and decreases towards NE and SW in the study area.

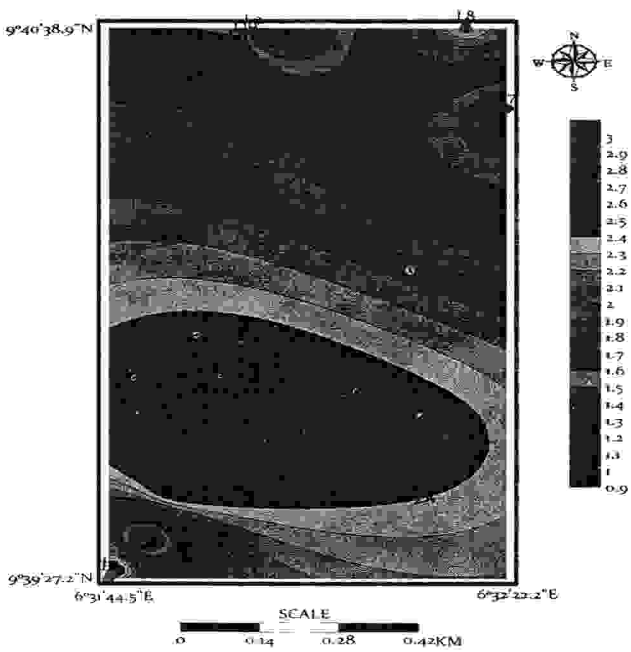

Figure 9. Fracture density map

Similarly, the surface fracture permeability values are highest in the central portion of the study area, but decreases towards NE and SW from there. Both surface fracture density and permeability are skewed roughly E-W.

Table 3 is the measured static water level data.

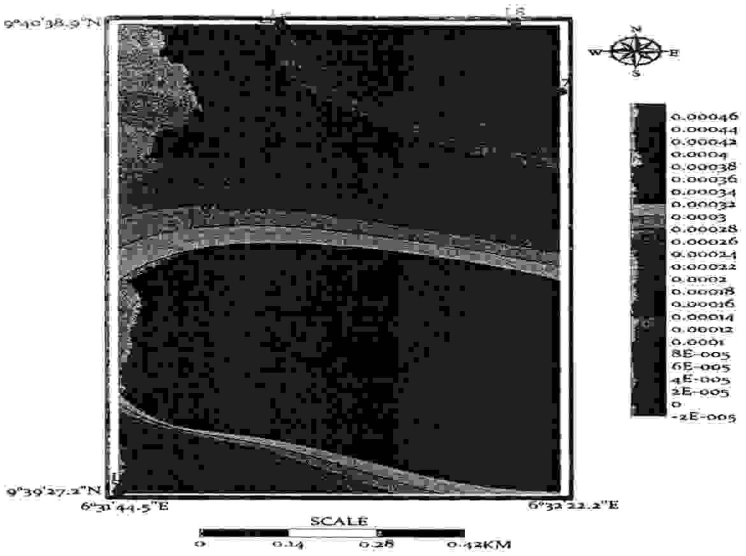

Figure 10. Surface fracture permeability

Table 3: Measured static water level data

LOCATION IDENTITY	SURFACE ELEVATION (m)	DEPTH TO STATIC WATER LEVEL (m)	STATIC LEVEL ELEVATION ((m)
L1	289	2	287
L2	293	1.7	290.3
L3	290	1.4	288.6
L4	294	1.9	292.1
L5	293	2.7	290.3
L6	295	3.4	291.6
L7	292	1.3	290.7
L8	290	0.8	289.2
L9	289	0.7	288.3
L10	293	0.6	292.4
L11	282	1.3	280.7
L12	287	1.1	285.9
L13	289	0.9	288.1
L14	284	1.2	282.8
L15	290	1.4	288.6
L16	285	0.8	284.2
L17	288	1.5	286.5
L18	289	1.8	287.2
L19	287	2.1	284.9
L20	294	1.3	292.7

Static water level elevation map (Fig.11) reveals two separate ridges on the static water level on the west of the study area. Both trend NW-SE in their southern portion, and then become N-S trending in their northern portion. In between the ridges is a clearly defined groundwater convergence zone within the regolith. This zone is configured N-S between L3 and L12 (western portion of Fig. 11). Olorunfemi and

Okhue (1992) observed that wells sited on static water level ridges commonly fail, while those sited on convergence zone are commonly very productive.

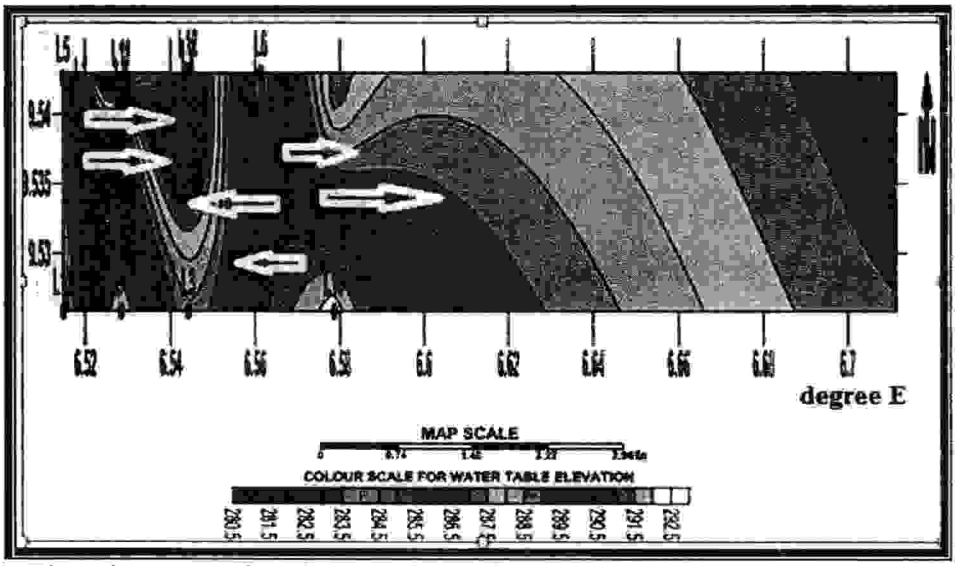

Figure 11. Elevation map of static water level showing water level ridges and flow direction

As expected, hand-dug wells almost sitting on the ridge (L4, L5, L6, and L10) are dry from January to April in the Dry season. Hand-dug wells within the convergence zone (L3, L11, L12, and L13) provide water from May to December. Hand-dug wells on the eastern portion of the study area are also productive, being located in the lower portion of the flow direction.

The convergence zone's coordinates coincides with the central portion with higher surface fracture density and permeability values. This suggests that surface fracture density and permeability data are useful in locating successful hand-dug wells.

Table 4 is the geographical coordinates of the vertical electrical sounding stations obtained with the GPS.

Table 4: Geographical coordinates of the vertical electrical sounding stations

N 9.65989	E 6.53	V1
N 9.6601	E 6.53	V2
N 9.56025	E 6.52997	V3
N 9.66044	E 6.5299	V4
N 9.6606	E 6.529944	V5
N 9.66077	E 6.529944	V6
N 9.660972	E 6.52992	V7
N 9.66117	E 6.52988	V8
N 9.6613	E 6.53	V9
N 9.6615	E 6.52988	V10
N 9.662	E 6.52991	V11
N 9.66175	E 6.52961	V12
N 9.66183	E 6.5294	V13
N 9.6621	E 6.52916	V14
N 9.66155	E 6.52944	V15
N 9.64611	E 6.52833	V16
N 9.64583	E 6.52847	V17
N 9.66166	E 6.52875	V18
N 9.66172	E 6.51222	V19
N 9.57783	E 6.54513	V20
N 9.57727	E 6.54458	V21
N 9.577388	E 6.5445	V22
N 9.57797	E 6.54563	V23

The vertical electrical resistivity sounding data at stations V1 to V11 is shown in table 5, and the corresponding data at stations V12 to V23 is shown in table 6. In the tables, AB is current electrode spacing, and ρ_a is measured apparent resistivity. The geo-electric layers and their respective depth and resistivity attributes modeled using *WinResist* are shown in tables 7 and 8. In the tables, htk, hρ, and htp respectively symbolizes, thickness, resistivity and layer type for layer h. ND implies not determined.

Table 5: Vertical electrical resistivity sounding data at stations V1 to V11

AB/2(m)	V1	V2	V3	V4	V5	V6	V7	V8	V9	V10	V11
	ρa (Ωm)	ρa (Ωm)	ρa (Ωm)	ρa (Ωm)	ρa (Ωm)	ρa (Ωm)	ρa (Ωm)	ρa (Ωm)	ρa (Ωm)	ρa (Ωm)	ρa (Ωm)
1	31	525	100	1716	305	1733	26	21	1937	345	300
2	20	361	109	1692	311	1897	19	19	1586	416	259
3	19	125	115	1853	332	2119	15	17	1186	466	141
5	34	125	110	1626	338	2194	14	15	956	584	416
6	10	209	106	1388	438	1977	12	12	769	650	626
8	30	158	95	1035	474	1492	12	14	631	627	578
10	10	241	74	734	467	936	15	15	538	694	523
15	62	210	51	545	531	838	19	18	452	646	332
20	77	227	39	467	547	762	28	22	409	605	357
25	51	280	64	561	653	640	15	17	407	495	379
30	79	159	48	437	601	530	22	21	349	457	227
35	362	115	35	413	596	474	27	23	356	431	213
40	519	243	21	437	658	426	31	35	449	413	183
50	148	159	12	500	358	577	34	50	675	160	77
60	368	181	16	549	259	587	45	69	597	112	77
70	186	303	11	592	121	528	65	99	727	61	56
80	231	-	17	526	258	537	49	53	-	139	-

Table 6: Vertical electrical resistivity sounding data at stations V12 to V23

AB/2(m)	V12	V13	V14	V15	V16	V17	V18	V19	V20	V21	V22	V23
	ρa (Ωm)	ρa (Ωm)	ρa (Ωm)	ρa (Ωm)	ρa (Ωm)	ρa (Ωm)	ρa (Ωm)	ρa (Ωm)	ρa (Ωm)	ρa (Ωm)	ρa (Ωm)	ρa (Ωm)
1	1854	653	400	29	23	3	372	310	525	1352	15	523
2	1428	582	233	23	26	3	286	228	367	1136	16	361
3	1190	263	122	19	30	2	228	141	115	834	17	125
5	826	192	108	15	32	2	233	142	135	667	20	125
6	790	174	116	12	31	2	99	176	140	612	22	158
8	619	149	114	9	32	2	123	197	234	512	20	241
10	554	145	205	8	32	2	146	107	227	414	19	230
15	608	134	215	10	27	2	130	431	217	405	22	227
20	765	154	310	11	27	2	172	367	280	455	27	280
25	484	136	214	6	23	2	169	438	164	406	23	159
30	604	153	321	6	16	2	296	367	105	437	28	115
35	745	161	444	6	13	2	284	215	170	524	31	174
40	945	161	330	7	10	3	268	284	238	712	40	243
50	819	178	184	9	9	4	196	235	148	904	45	159
60	786	218	113	10	14	4	382	224	313	1042	61	303
70	819	267	-	14	12	6	970	280	-	1087	58	-
80	732	172	-	8	-	5	-	-	-	1045	78	-

Table 7: Geo-electric layers modeled from data collected at stations V1 to V11 using *WinResist*

GEOELETRIC LAYER	V1	V2	V3	V4	V5	V6	V7	V8	V9	V10	V11
h1 tk	1.1	0.8	0.7	0.9	2.6	2.0	0.7	5.0	3.9	1.3	0.6
h1ρ	34.8	757.3	93.3	1590	299.1	305	29.3	21	1472	334	416
h 1 tp	TS	TS	TS	TS	TS	TS	TS	TS	TS	TS	TS
h 2 tk	2.5	1.5	9.0	0.9	13	8	7.6	5.0	6.6	8.3	0.8
h2ρ	10.2	70.7	141.3	2794.7	1379	467	11.5	15	64.4	1392	95
h 2 tp	WB	WB	FB	FB	FB	WB	WB	WB	WB	FB	WB
h 3 tk	80.4	2.8	37.5	17.4	44.4	15	4.7	10	50.3	47	2.8
h3ρ	6516.7	401	64.7	399.7	56.9	653	30.6	22	6120	51	1622
h 3 tp	FB	FB	FR	FR	FR	FB	FB	FB	FB	FR	FB
h 4 tk	9.6	20.4	ND	4.9	257	45	4.6	5.0	9.1	ND	8.7
h4ρ	161.2	92.2	26.9	531.5	ND	121	16.4	17	809	194	43
h 4 tp	FR	FR	-	FB	FB	FB	FB	FR	FR	FB	FR
h 5 tk	10.2	4.6	-	9.7	-	ND	62.2	45	ND	-	-
h5ρ	389.2	256	-	464.7	-	258	206.5	99	1656	-	-
h 5 tp	FB	FB	-	FR	-	FB	FB	FB	FB	-	-
h 6 tk	9.9	ND	-	36	-	-	10	9.3	-	-	-
h6ρ	193.2	671	-	779.5	-	-	66.7	58	-	-	-
h 6 tp	FR	FB	-	FB	-	-	FB	FR	-	-	-
h 7 tk	ND	-	-	13.6	-	-	-	-	-	-	-
h7ρ	277.1	-	-	585.1	-	-	-	-	-	-	-
h 7 tp	FB	-	-	FR	-	-	-	-	-	-	-
h 8 tk	-	-	-	-	-	-	-	-	-	-	-
h8ρ	-	-	-	-	-	-	-	-	-	-	-
h 8 tp	-	-	-	-	-	-	-	-	-	-	-
Curve type	HKHKH	HKHK	KQ	KHKHK	KH	AKH	HKHK	HKHK	HKH	KH	HK

TS, WB, FB, FR respectively symbolizes top soil, weathered basement, and fractured basement in tables 7 and 8.

Table 8: Geo-electric layers modeled from data collected at stations V12 to V23 using *WinResist*

GEOELETRIC LAYER	V12	V13	V14	V15	V16	V17	V18	V19	V20	V21	V22	V23
h1 tk	1.6	1.1	0.8	1.5	1.5	0.8	1.3	0.9	0.7	0.8	2.1	1.3
h1ρ	1792	728	515	29	23.5	3	366	370	533	759	1231	15
h 1 tp	TS	TS	TS	TS	TS	TS	TS	TS	TS	TS	TS	TS
h 2 tk	10.5	17.6	3.2	12.7	8.4	22.6	4.3	4	2.7	1.6	10.9	17.6
h2ρ	522	118	185	3	40	2	65	221	139	70	335	21
h 2 tp	FB	WB	WB	WB	FB	WB	WB	WB	WB	WB	WB	WB
h 3 tk	9.4	50.6	6.6	50.6	25	40	ND	4.5	12.5	2.7	45	40.2
h3ρ	968	348	952	22	7	18	4007	994	621	560	4608	264
h 3 tp	FB	FB	FB	FB	FR	FB	FB	FB	FB	FB	FB	FB
h 4 tk	4.6	11.6	7.8	12.5	ND	9.4	-	17	19	6.3	6.5	9.1
h4ρ	579	174	26	11	22.5	10	-	142	91	95	1479	74
h 4 tp	FR	FR	FR	FR	FB	FR	-	FR	FR	FR	FR	FR
h 5 tk	15.2	-	-	-	-	-	-	4.6	10	3.5	-	ND
h5ρ	1193	-	-	-	-	-	-	207	244	159	-	156
h 5 tp	FB	-	-	-	-	-	-	FB	FB	FB	-	FB
h 6 tk	19.9	-	-	-	-	-	-	22	15	7.5	-	-
h6ρ	752	-	-	-	-	-	-	124	216	109	-	-
h 6 tp	FR	-	-	-	-	-	-	FR	FR	FB	-	-
h 7 tk	10	-	-	-	-	-	-	ND	-	9.3	-	-
h7ρ	797	-	-	-	-	-	-	211	-	338	-	-
h 7 tp	FB	-	-	-	-	-	-	FB	-	FB	-	-
h 8 tk	11.2	-	-	-	-	-	-	-	-	8	-	-
h8ρ	681	-	-	-	-	-	-	-	-	228.5	-	-
h 8 tp	FR	-	-	-	-	-	-	-	-	FR	-	-
h9ρ	-	-	-	-	-	-	-	-	-	607	-	-
Curve type	HKHKHK	HK	HK	HK	KH	HK	H	HKHKH	HKHKHKH	HK	AKH	HKHKHKH

The curve types are mostly combination of H and K curves. Four geoelectric layers constitute the curve with the highest frequency. The curve type was found at ten stations (V3, V5, V10, V11, V13, V14, V15, V16, V17 and V18). The KH generally contains thick and deep fracture intervals characterized with low resistivity values in the study area (tables 7 and 8). Similar deep fractures are associated with five layer-, six layer-, and seven layer curve-types in the study area. Some of the curves that display fracture intervals deeper than 50m are figures 12 and 13.

The curve types are mostly combination of H and K curves. Four geoelectric layers constitute the curve with the highest frequency. The curve type was found at ten stations (V3, V5, V10, V11, V13, V14, V15, V16, V17 and V18). The KH generally contains thick and deep fracture intervals characterized with low resistivity values in the study area (tables 7 and 8). Similar deep fractures are associated with five layer-, six layer-, and seven layer curve-types in the study area.

Some of the curves that display fracture intervals deeper than 50m are figures 12 and 13.

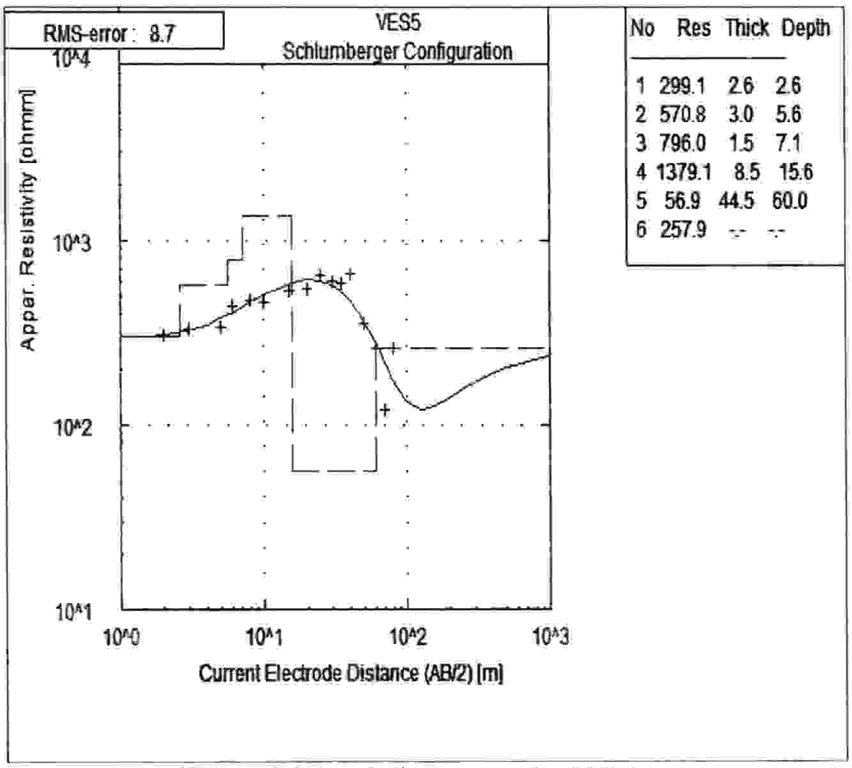

Figure 12. Modelled curve for V5 data

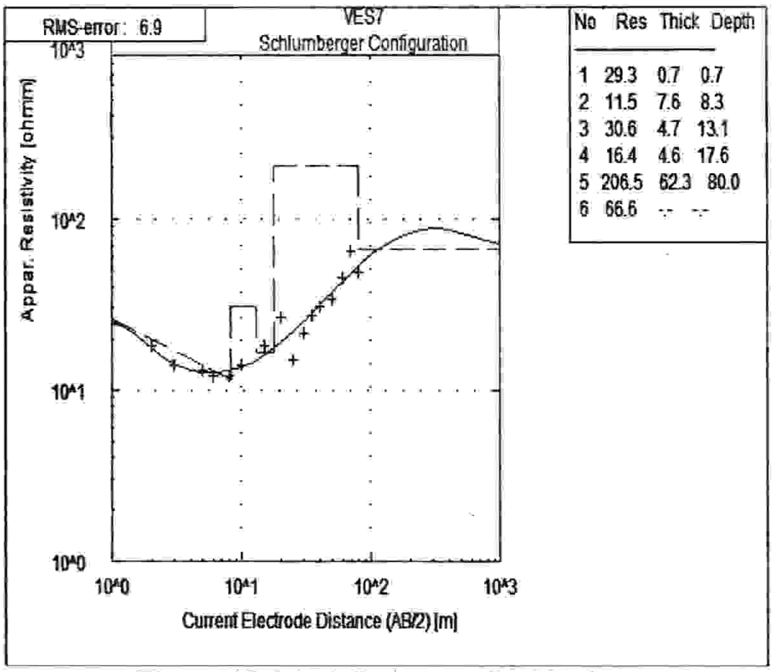

Figure 13. Modelled curve for V7 data

Values of S, T, λ for fractures existing within the depth interval 50-70m are given in table 9, and those for fractures existing within the depth interval 70-85m are given in table 10. High λ values (0.9999 to 1.0001) and low S (0.0044 to 0.23mS) generally indicate that the low resistivity anomaly at intervals deeper than 50m are associated with deep water-filled fractures. Moderate to high values of T (1000 to 5000 Ωm^2) also indicate high secondary permeability in basement complex. This interpretation is consonant with the findings of many workers (Olorunfemi and Oloruniwo, 1985; Olorunfemi *et al.*, 1991; Oladapo *et al.*, 2004; Sunmonu *et al.*, 2012; Oladunjoye *et al.*, 2013; Ayuk *et al.*, 2013; Kumar *et al.*, 2014). Low λ (0.756), high S (0.566) and low T (89.3 Ωm^2) at V17 indicate that the very low resistivity anomalous value (lower than 10 Ωm in Fig.14) is unlikely to be associated with fracturing. It is probably produced by the presence of electronically conductive minerals.

Table 9: Values of S, T, λ for fractures existing within the depth interval 50-70m

STATION	S	T	Λ
4	0.23	7957.4	0.995
5	0.782	2526.4	1.00
6	0.372	5445	1.0001
9	0.011	7358	0.9886
10	0.9197	2401	0.9996
12	0.026	14974	0.991
17	0.5666	89.83	0.7567
19	0.1778	2721.4	0.9998
20	0.0708	3301.7	0.9993
22	0.0044	9612.8	1.000
23	0.12347	670.7	0.999

Table 10: Values of S, T, λ for fractures existing within the depth interval 70-85m

STATION	S	T	λ
1	0.0595	1547.5	0.9995
4	0.023	7957.4	0.995
7	0.1499	667	0.999
8	0.1603	539.4	0.999
12	0.0165	7624.96	1.000
13	1.1792	132.5	0.999

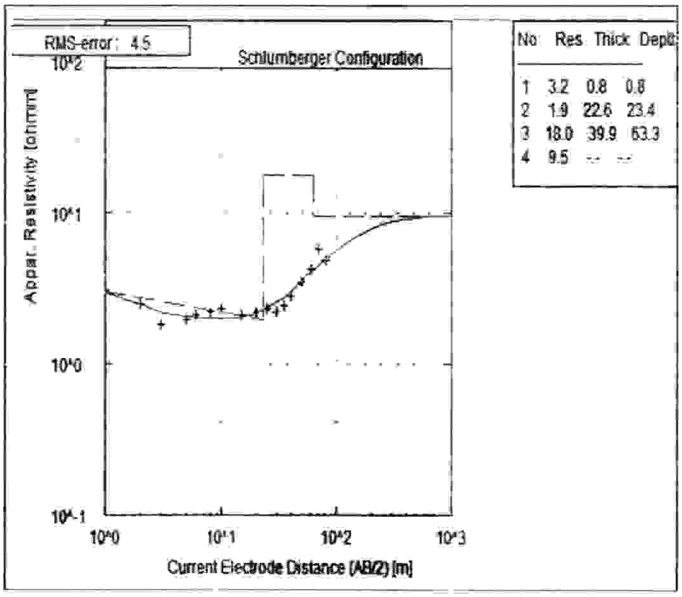

Figure 14. Modelled curve for V17 data

Isoresistivity, thickness, λ, S and T attribute maps for fracture intervals between 50 to 70 m depth are respectively figures in 15, 16, 17, 18 and 19.

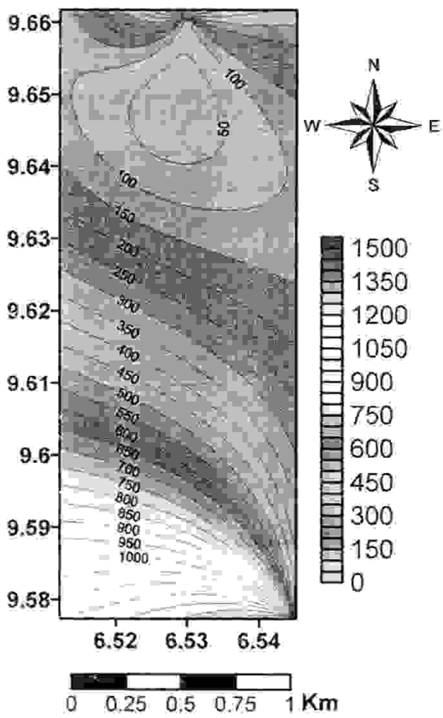

Figure 15. Isoresistivity map for fractures within 50-70m depth interval

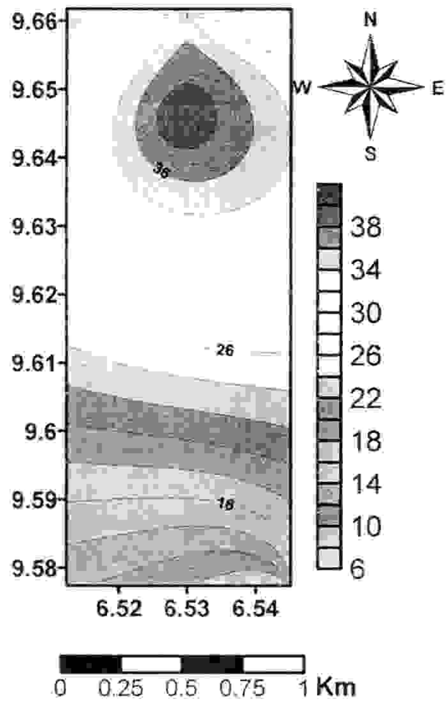

Figure 16. Thickness map for fractures within 50-70m depth interval

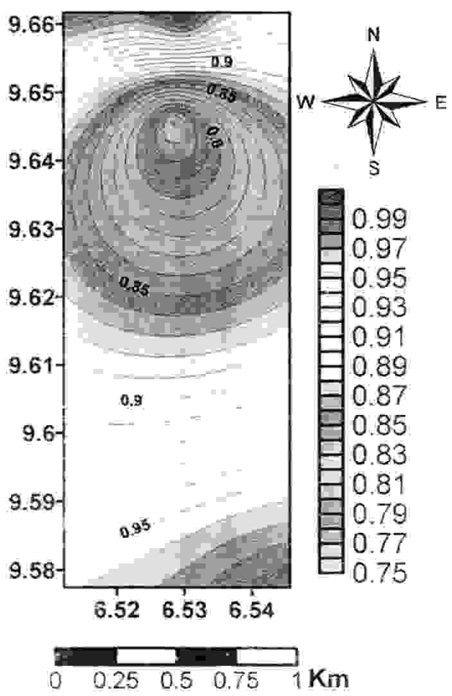

Figure 17. λ map for fractures within 50-70m depth interval

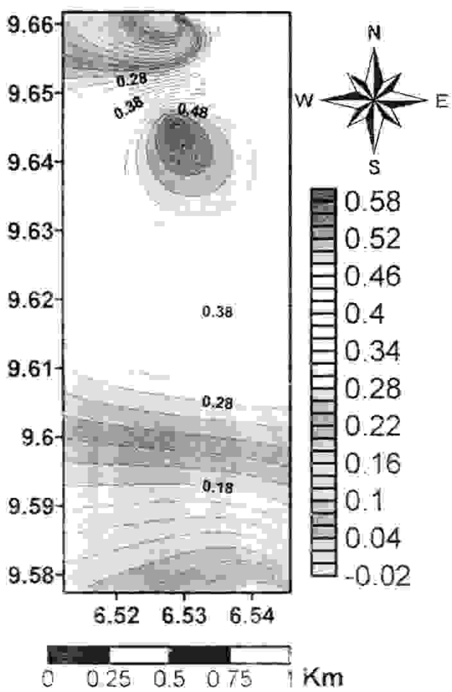

Figure 18. S map for fractures within 50-70m depth interval

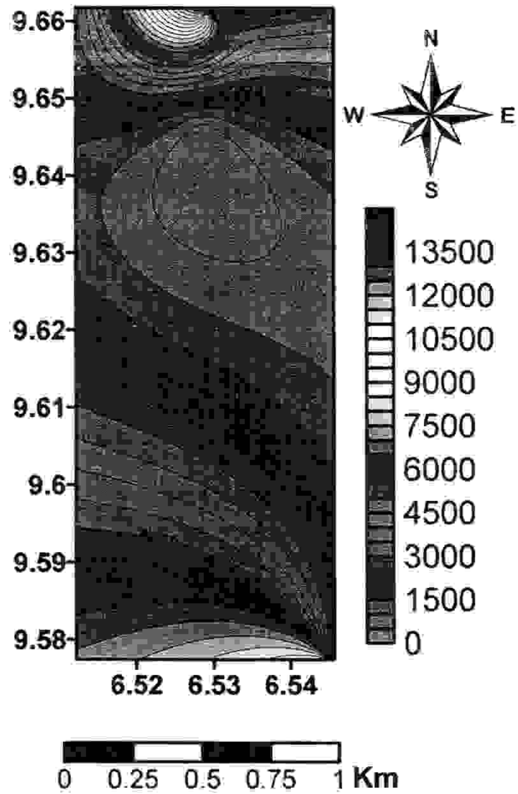

Figure 19. T map for fractures within 50-70m depth interval

Figures 15, 16, 17, 18 and 19 show that the northeastern and northwestern portions of the study area ,within latitudes N9.645° to N9.665°, posses subsurface fractures with optimum attributes for supporting continual water production. These fractures are characterized with resistivity values ranging from 100-300Ωm, fracture thickness ranging from 24 to 32m, electrical anisotropy higher than 0.95, longitudinal unit conductance values lower than 0.1Ω-1 and transverse unit resistance between 2000 and 6000Ωm2.

CONCLUSION

Elevation of static water level constitutes direct hydrogeological data deployed to establish a groundwater convergence zone between two water level ridges. Hand-dug wells within the convergence zone are continually productive. Those within the vicinity of the convergence zone are unproductive in the Dry season. The groundwater convergence zone lies within the central portion of the area where surface fracture density and permeability are high. Surface fracture density and permeability data are thus shown to be effective information for locating productive hand-dug wells.

Resistivity anomalies were evaluated using electrical anisotropy, longitudinal unit conductance and transverse unit resistance. This revealed the existence of deep fractures with optimum attributes for supporting steady water production in northeastern and northwestern portions of the study area within the region between latitudes N9.645° to N9.665°.

REFERENCES

Bhattacharya, P.K. and Patra, H.P. (1968). Direct Current Geoelectric Sounding. Elsevier London, p. 574.

Brace, W.F. (1980). Permeability of crystalline and argillaceous rocks. International Journal of Rock Mechanics and Material Science, 17, pp. 241-245.

Chandra, S., Rao, V.A., Krishnamurthy, S., and Ahmed, A.S., (2006). Integrated studies for characterization of lineaments used to locate groundwater potential zones in a hard rock region of Karnataka, India. Hydrogeology Journal, Vol.14, pp. 1042-1051.

Deming, D. (2002). Introduction to Hydrogeology (1st Edition), McGraw Hills, New York, p. 468.

Henriet, J.P. (1976). Direct applications of the Dar Zarrouk parameters in groundwater surveys. Geophysical prospecting, Vol. 24.

Kumar, D., Rai, S.N., Thiagartan, S., and Kumari, Y.R., (2014). Evaluation of heterogeneous aquifers in hard rocks from resistivity sounding in parts of Kalmeshwar taluk of Nagpur district, India. Current science, Vol. 107 (7), pp.1139-1145.

Mallam, A. and Emenike, E.A. (2008). Preliminary findings of subsurface characteristics from direct current resistivity survey of the Federal Capital Territory(FCT) Nigeria. International journal of pure and applied science 2(2): pp. 68-76.

Oladapo, M.I., Mohammed, M.Z, Adeoye, O.O., and Adetola, B.A. (2004). Geoelectrical investigation of Ondo State Housing Corporation Estate Ijapo Akure, southwestern Nigeria. Journal of mining and geology, Vol.4 (1), pp. 41-48.

Olorunfemi , M.O. (2009). Groundwater exploration,borehole site selection, and optimum drill depth in Basment Complex terrain. Special publication series 1, Water Resources, p. 19.

Olorunfemi, M.O. and Idornigie, A.T. (1992). A geoelectric mapping of basement structures of south-central part of Bida Basin and its hydr logical implication. Journal of mining and geology, Vol. 28 (2), pp. 98-94.

Olorunfemi, M.O. and Okhue, E.T. (1992). Hdrogeologic and geologic significance of a geoelectrical survey at Ile-Ife, Nigeria. Journal of mimning and geology, Vol 28(2), pp. 79-89.

Olorunfemi, M.O. and Oloruniwo, M.A. (1985). Geoelectric parameters and aquifer characteristics of some parta of southwestern Nigeria.Geologia Applicata E,I diogeologia,XX, part 1, pp.90-99.

Olorunfemi, M.O., Ojo, J.S., and Oladapo, M.I. (1998). Geological, Hydrogeological, and Geophysical Investigations of Exposed 20" Excravos Lagos Pipiline Technical Report.

Olorunfemi, M.O., Olanrewaju, V.O. and Alade,O. (1991). On the electrical anisotropy and groundwater yield in a Basment Conmplex area of southwestern Nigeria. Journal of African earth sciences, Vol12(3), pp. 467-472.

Oyedele, E.A.A, Oyedele, T., and Oyedele, K. (2013). Geoelectrical data analysis todemarcate groundwater pockets in Ado-Ekiti, southwest Nigeria. International Journal of Water Resources and Environmental Engineering, pp. 609-615.

Parasnis, D.S. (1986). Principles of Applied Geophysics (4th Edition), Chapman and Hall, New York, p. 383.

Sinha, R, Israil, M., and Singhal, D.C. (2009). A hydrogeophysical model of the relationship between geoelectric and hydraulic parameters of anisotropic aquifers. Hydrogeology Journal, Vol. 17, pp. 495-503.

Sonkambe, S., Chandra, S, Nagaiah, E, Dar, F.A., Somvanshi, V.K. and Ahmed, S. (2013). Arabian Journal of Geosciences, pp. 1-4.

Sumonu,L.A., Adagunodu,T.A., Olafisoye, E.R., and Oladapo, O.P. 2012. The groundwater potential evaluation at industrial estate, Ogbomosho, southwestern Nigeria. Materials and geoenvironment, Vol 54(4), pp. 363-390.

Unuevho, C,Onuoha,K.,M., and Alkali, Y.,B., 2012. Direct current resistivity methods for groundwater prospecting in hardrock terrains: A viable approach to providing sustainable potable water. CHSUDJ Vol.3 (1) pp. 1-16.